Electronic Supplementary Material (ESI) for Journal of Materials Chemistry A.

Aqueous- and vapor-phase detection of nitroaromatic explosives by a water-stable fluorescent microporous MOF directed by ionic liquid

Jianhua Qin,[a,b] Bing Ma,[a] Xiao-Fei Liu,[a] Hong-Lin Lu,[a] Xi-Yan Dong,[a] Shuang-Quan Zang*[a] and Hongwei Hou*[a]

[a] *College of Chemistry and Molecular Engineering, Zhengzhou University, Zhengzhou 450001, China.*

[b] *College of Chemistry and Chemical Engineering, Luoyang Normal University, Luoyang 471022, China.*

Author for correspondence:

Prof. S.-Q. Zang, E-mail: zangsqzg@zzu.edu.cn;

Prof. H.-W. Hou, E-mail: houhongw@zzu.edu.cn.

Supporting Information

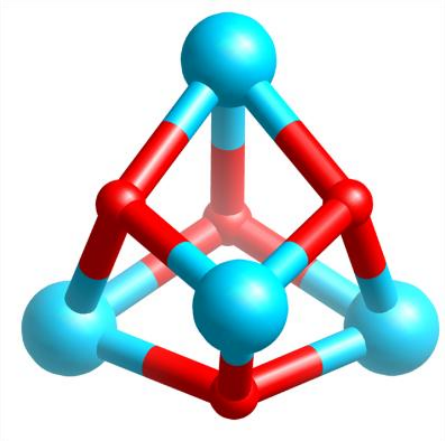

Fig. S1 View of the cubane-shaped tetranuclear $[Tb_4(\mu_3\text{-}OH)_4]^{8+}$ cluster.

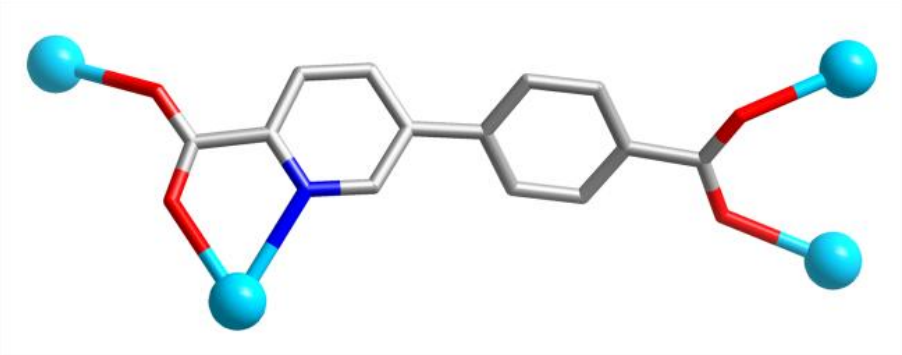

Fig. S2 Coordination mode of L ligand.

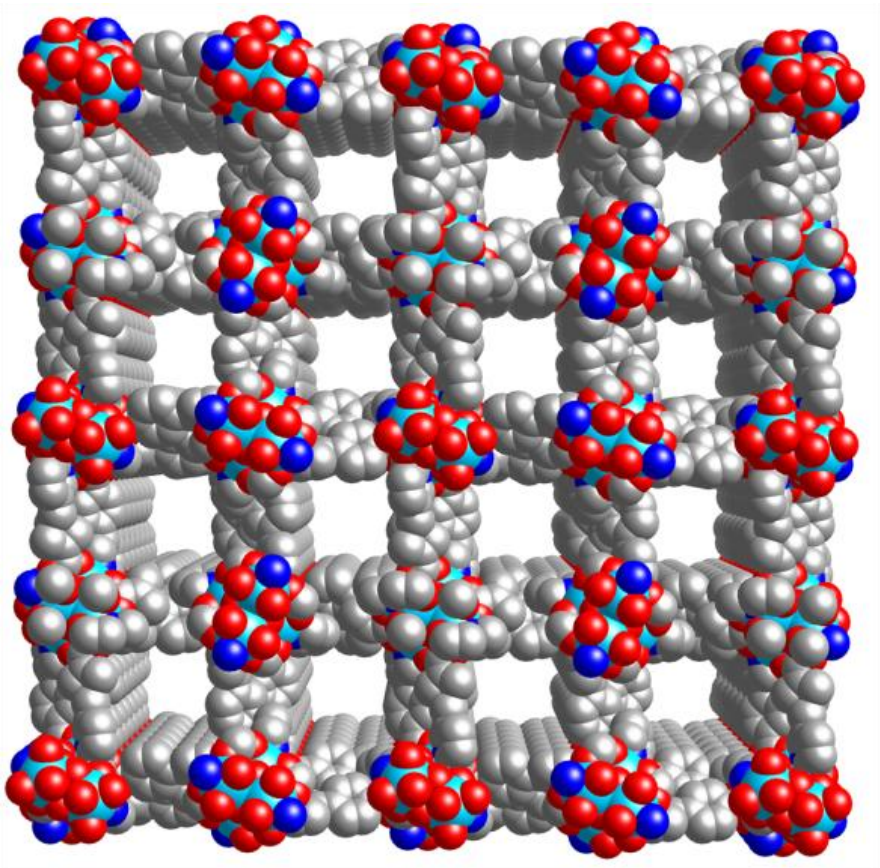

Fig. S3 Space-filling model to show the channels along the *c*-axis direction.

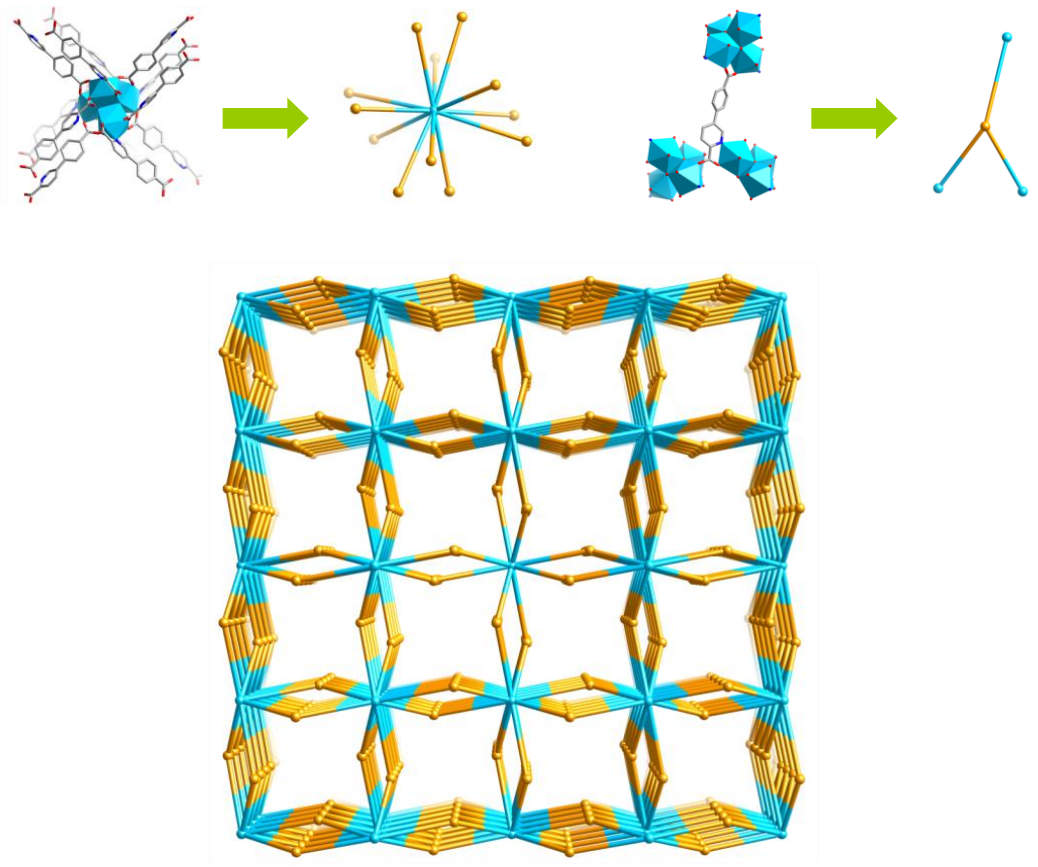

Fig. S4 Schematic representation of the (3,12)-connected ($4^{20}.6^{28}.8^{18}$)(4^{3})$_4$ topology. The topological net of **1**. (Node: Tb4 cluster, turquoise, 12-connected node; L ligand, light orange, 3-connected node)

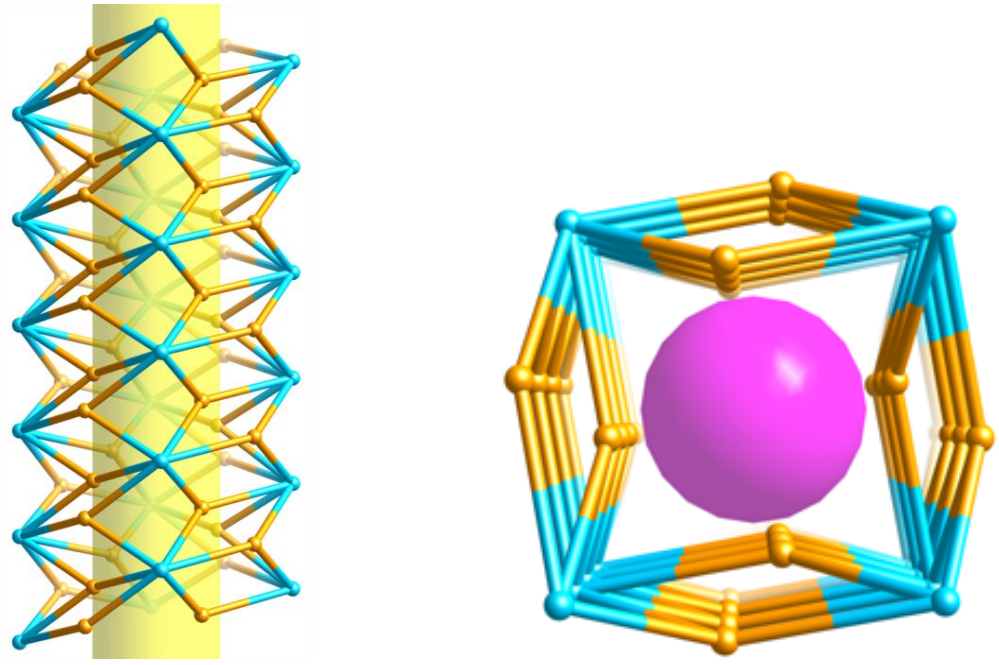

Fig. S5 The 1D channel.

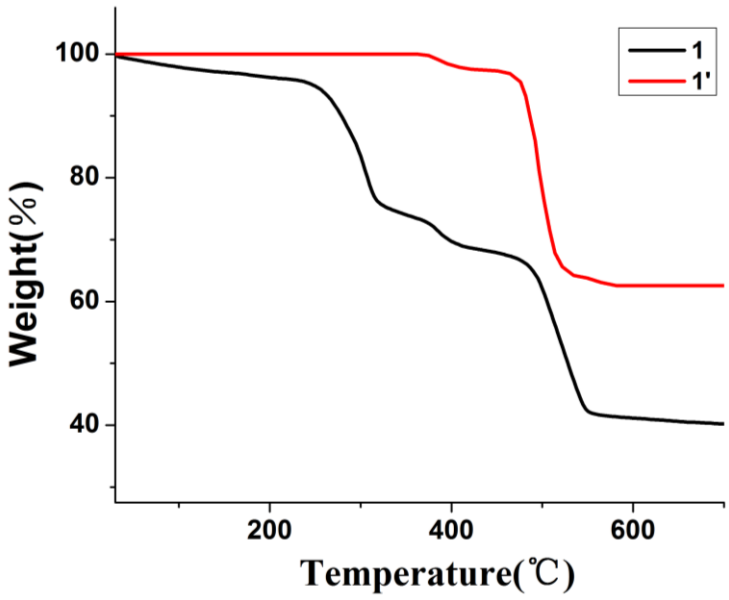

Fig. S6 Thermogravimetric curve of **1** and **1'**. Based on the combination of SQUEEZE calculations assist with the TG and EA analyses, the tentative formula can be given as $[Tb(L)(OH)]\cdot 2(H_2O)\cdot 0.5(DMF)$.

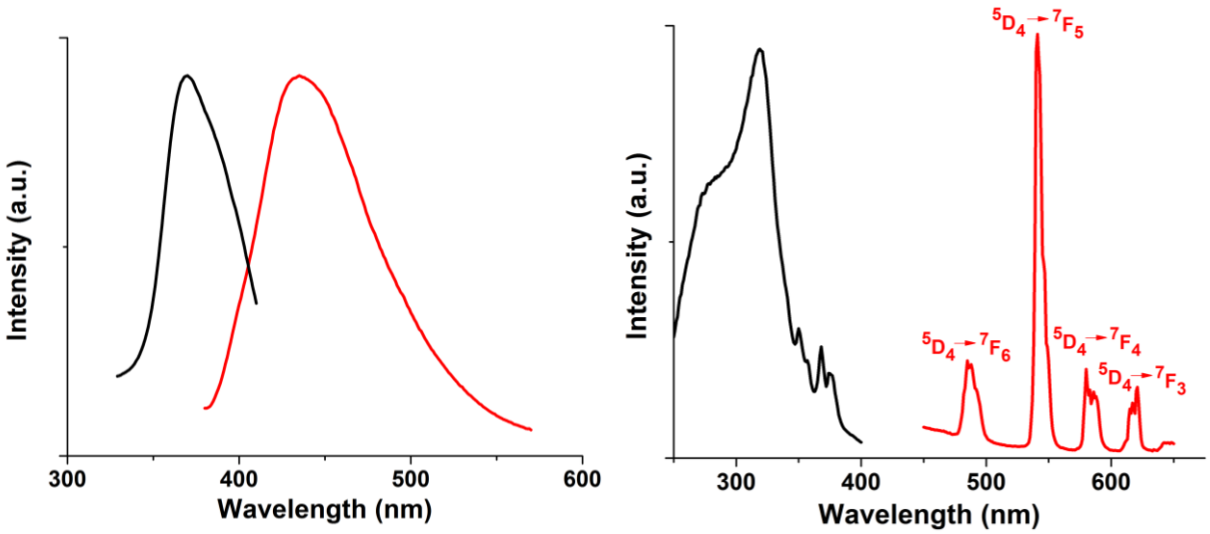

(a) (b)

Fig. S7 Solid-state excitation and emission spectra for H_2L (a) and **1'** (b**)** at room temperature.

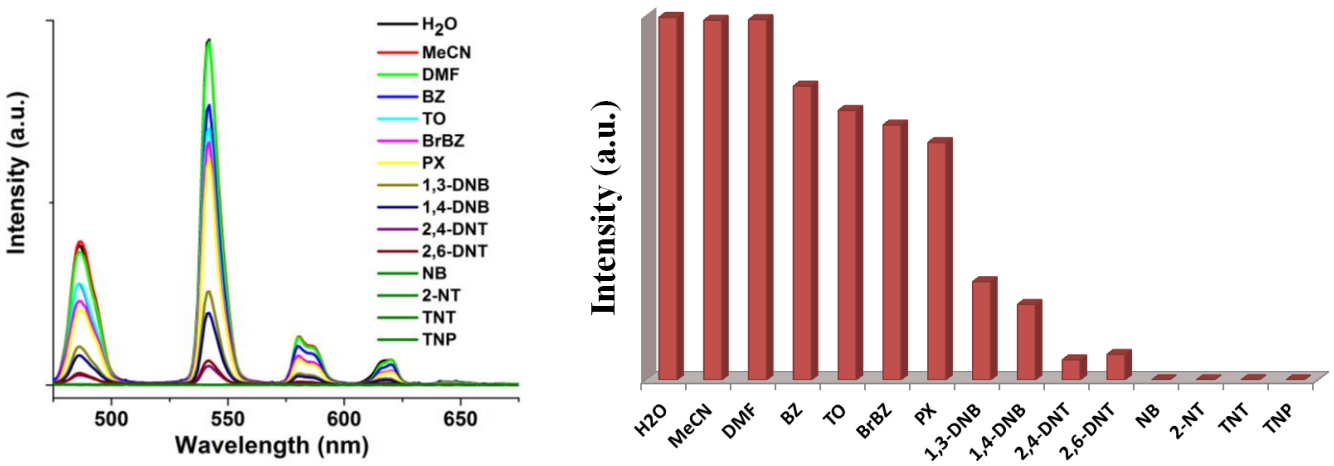

(a) (b)

Fig. S8 The emission spectra (a) and the fluorescent intensity (b) for **1'** dispersed in H_2O, MeCN, DMF, BZ, TO, BrBZ, PX, and 1 mM or saturated aqueous solutions of eight different analytes at room temperature.

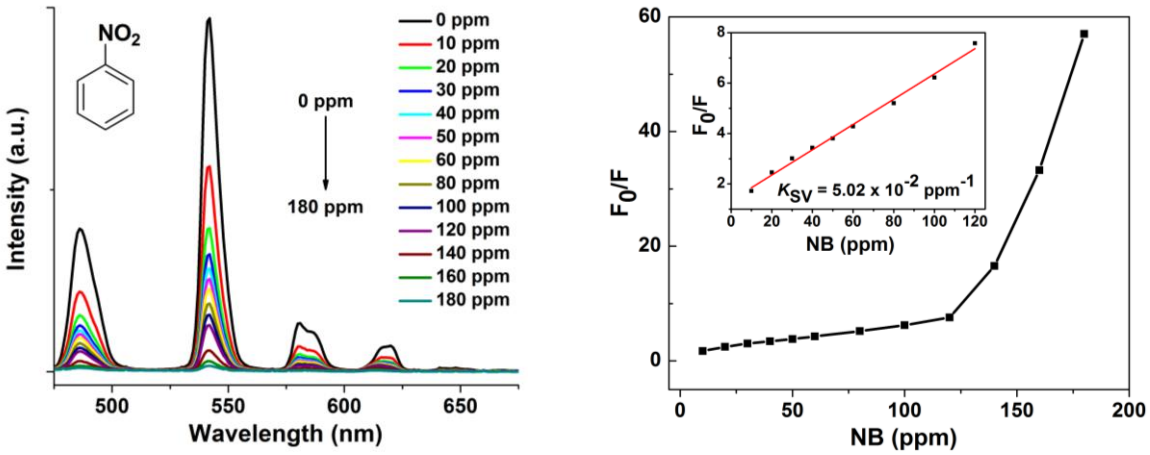

(a) (b)

Fig. S9 (a) Fluorescence titration of **1'** dispersed in aqueous solution by gradual addition of NB.

(b) Stern-Volmer plot of F_0/F *vs.* NB concentration in aqueous solution for **1'**.

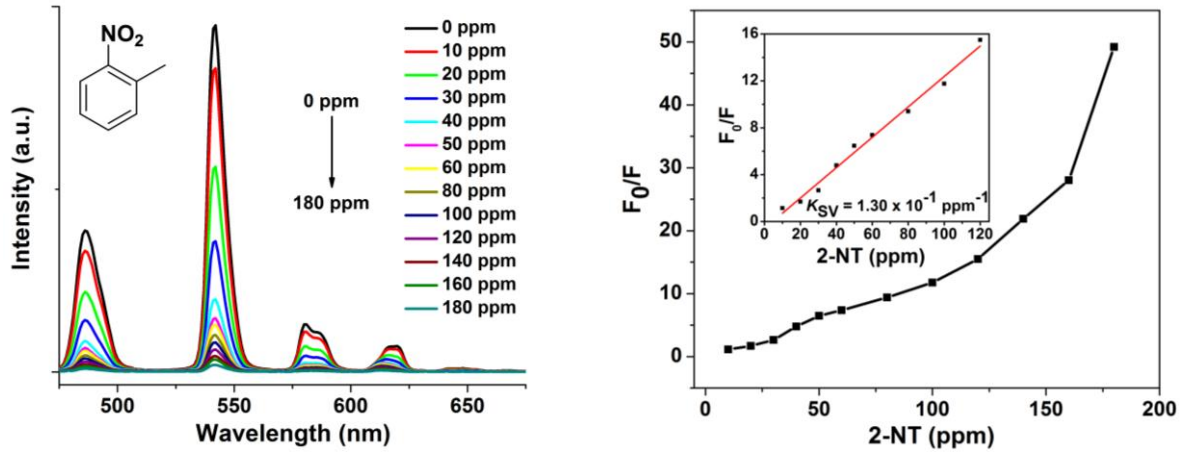

(a) (b)

Fig. S10 (a) Fluorescence titration of **1'** dispersed in aqueous solution by gradual addition of 2-NT.

(b) Stern-Volmer plot of F_0/F *vs.* 2-NT concentration in aqueous solution for **1'**.

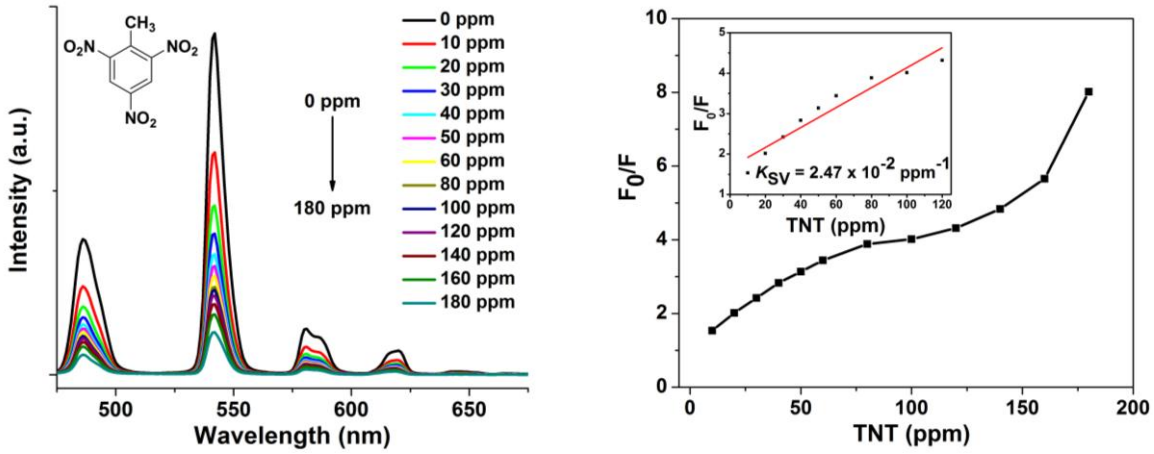

(a) (b)

Fig. S11 (a) Fluorescence titration of **1'** dispersed in aqueous solution by gradual addition of TNT.

(b) Stern-Volmer plot of F_0/F *vs.* TNT concentration in aqueous solution for **1'**.

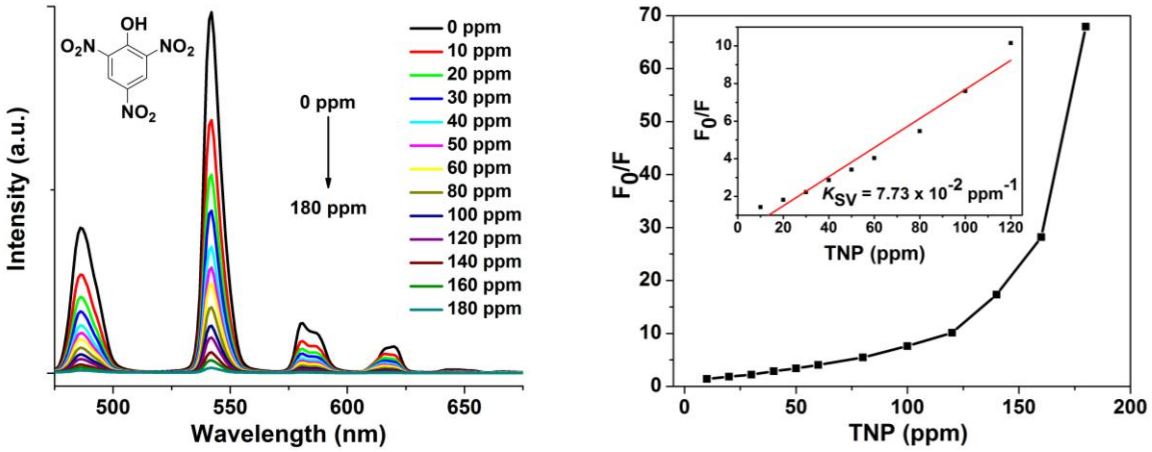

(a) (b)

Fig. S12 (a) Fluorescence titration of **1'** dispersed in aqueous solution by gradual addition of TNP. (b) Stern-Volmer plot of F_0/F *vs.* TNP concentration in aqueous solution for **1'**.

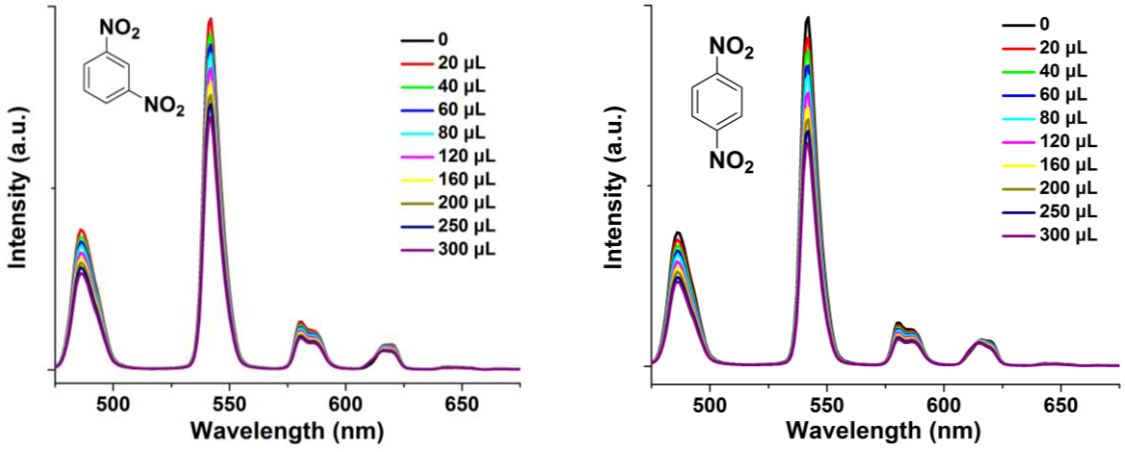

(a) (b)

Fig. S13 Fluorescence titration of **1'** dispersed in aqueous solution by gradual addition of saturated aqueous solutions of 1,3-DNB (a) and 1,4-DNB (b).

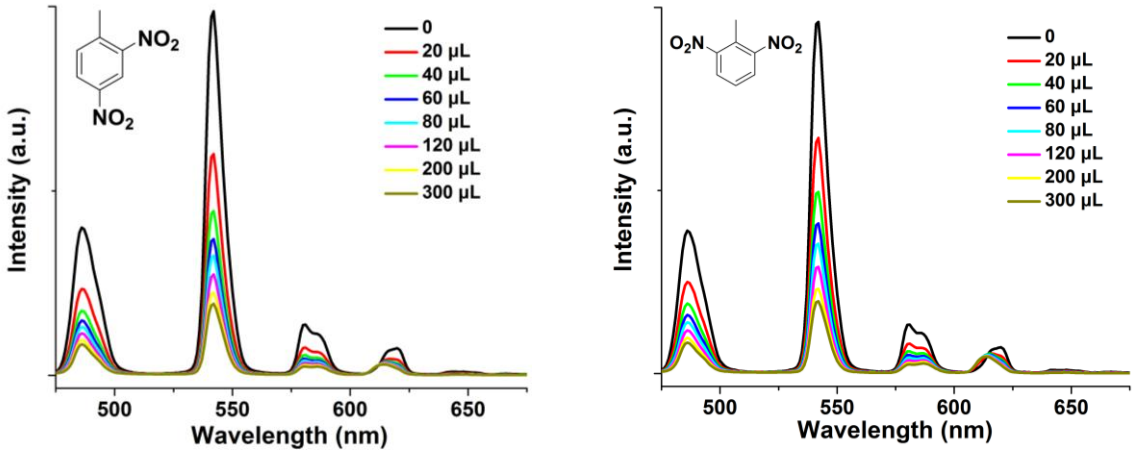

(a) (b)

Fig. S14 Fluorescence titration of **1'** dispersed in aqueous solution by gradual addition of saturated aqueous solutions of 2,4-DNT (a) and 2,6-DNT (b).

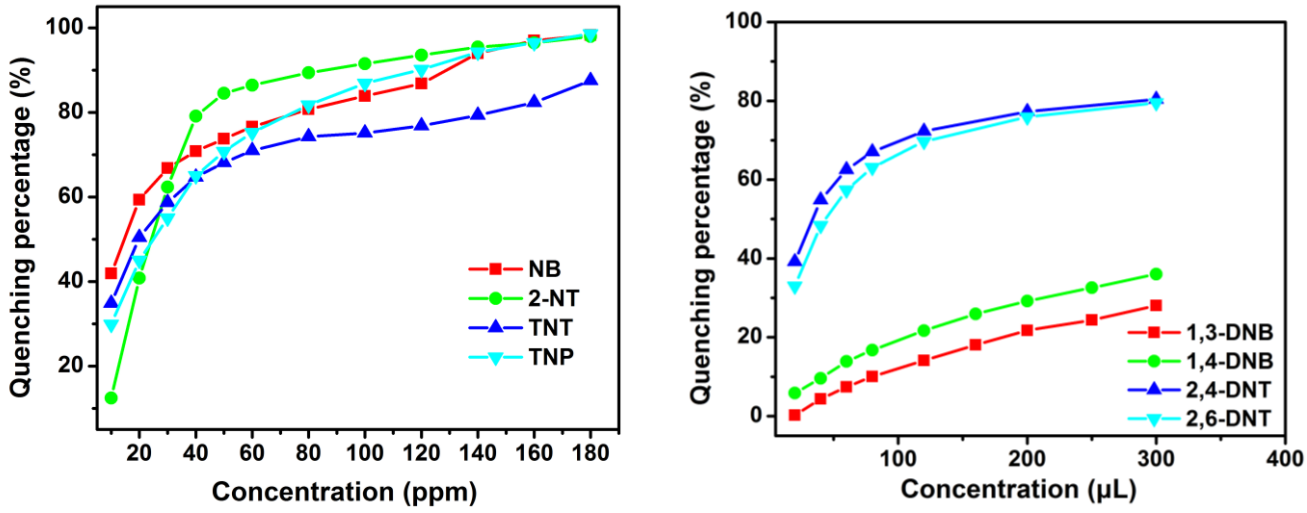

(a) (b)

Fig. S15 (a) Plot of quenching efficiency of **1'** dispersed in aqueous solutions at different concentrations of NB, 2-NT, TNT, and TNP. (b) Plot of quenching efficiency of **1'** dispersed in aqueous solutions upon incremental addition of saturated aqueous solutions of 1,3-DNB, 1,4-DNB, 2,4-DNT, and 2,6-DNT.

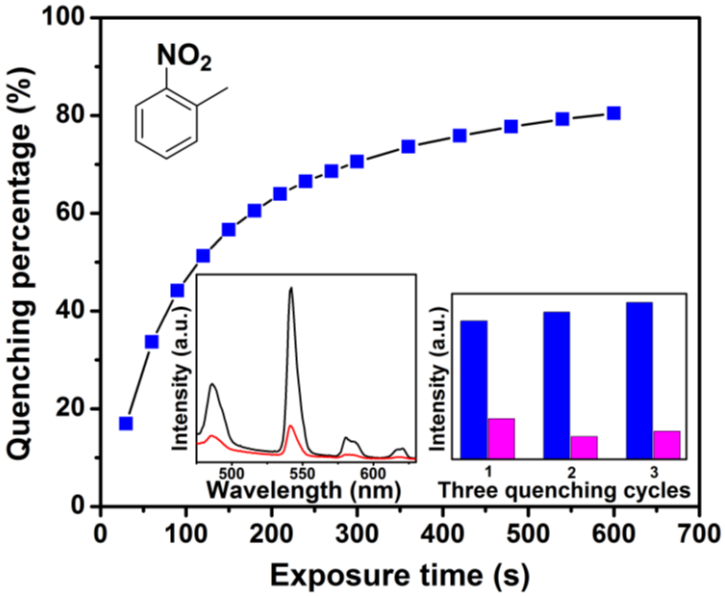

Fig. S16 The time-dependent fluorescence quenching upon exposure to 2-NT vapor. Insets: (left) corresponding emission spectra before and after exposure of **1'** to the 2-NT vapor for ten minutes; (right) results for three continuous quenching cycles.

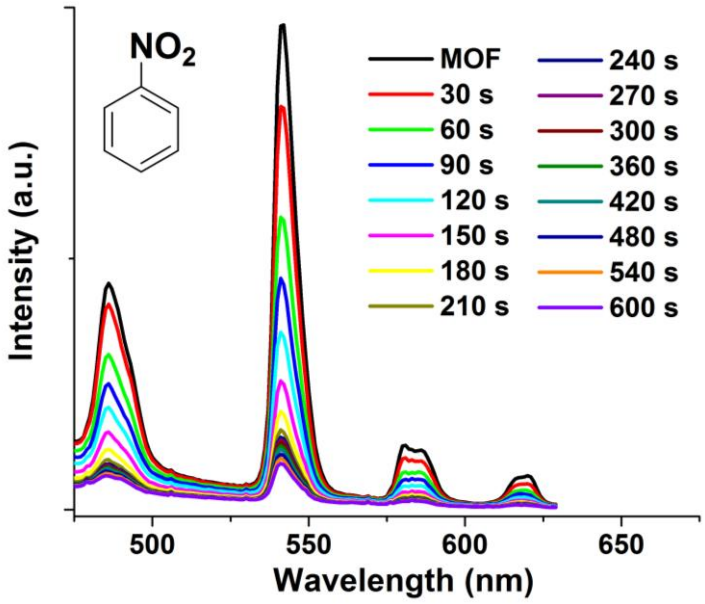

Fig. S17 The time-dependent emission spectra of **1'** upon exposure to NB vapor.

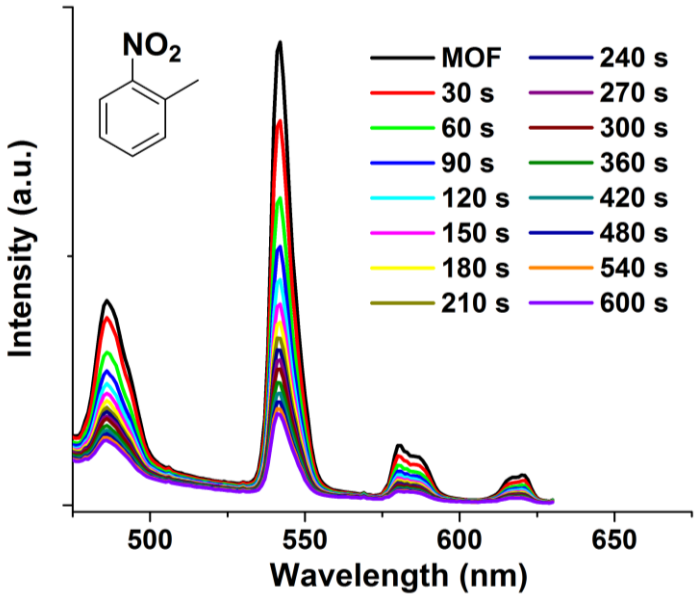

Fig. S18 The time-dependent emission spectra of **1'** upon exposure to 2-NT vapor.

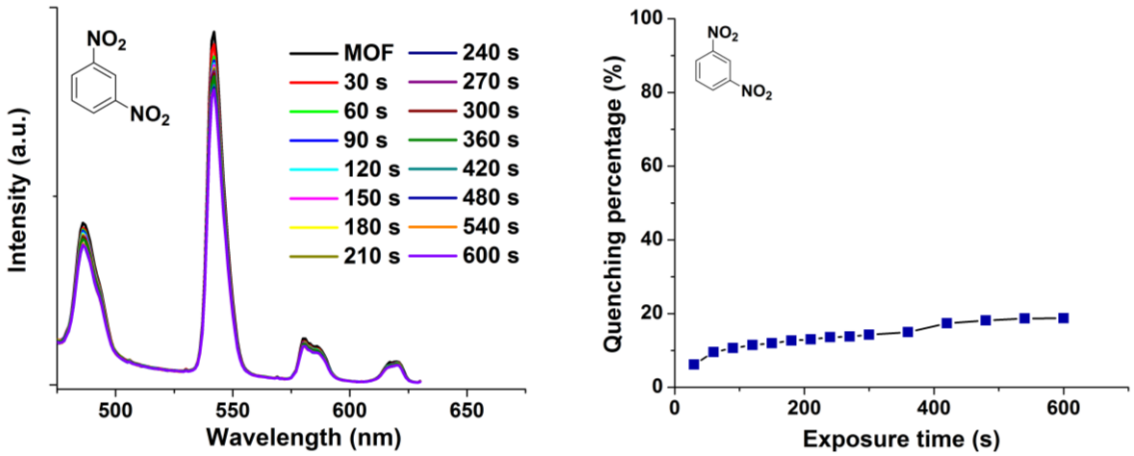

Fig. S19 The time-dependent emission spectra (a) and fluorescence quenching (b) of **1'** upon exposure to 1,3-DNB vapor.

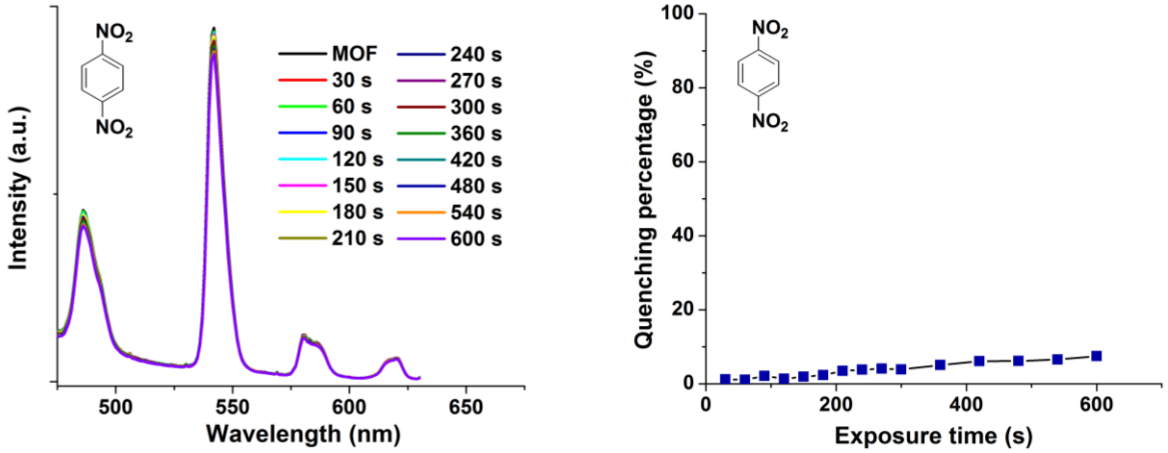

(a) (b)

Fig. S20 The time-dependent emission spectra (a) and fluorescence quenching (b) of **1'** upon exposure to 1,4-DNB vapor.

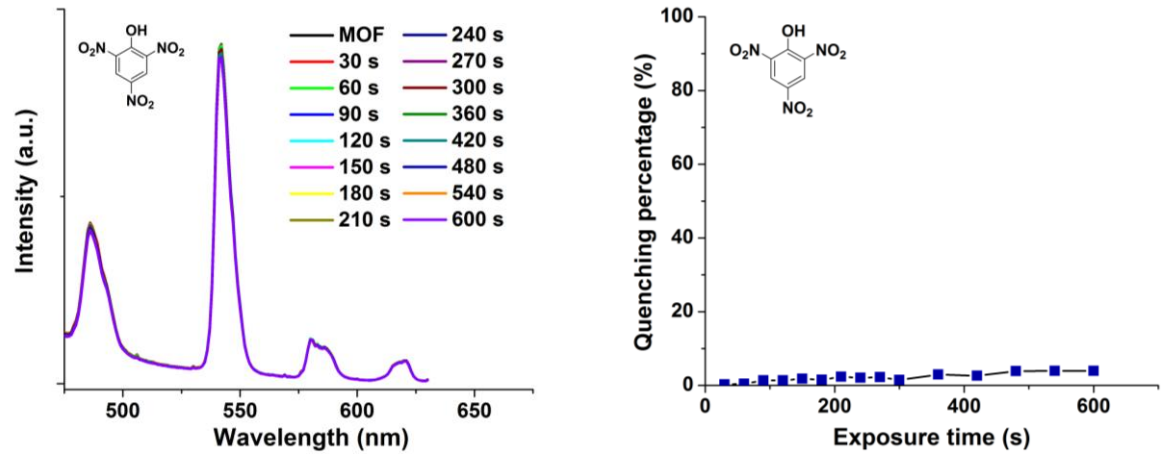

(a) (b)

Fig. S21 The time-dependent emission spectra (a) and fluorescence quenching (b) of **1'** upon exposure to TNP vapor.

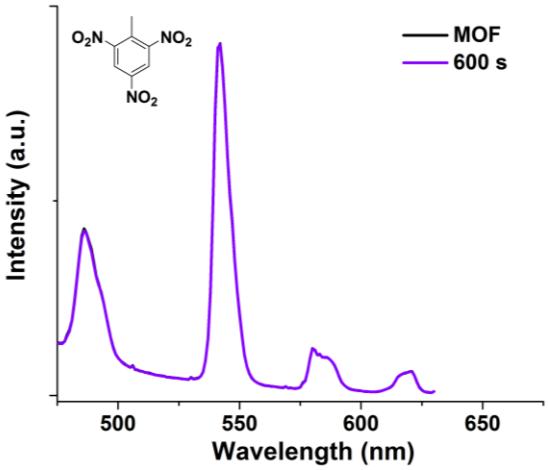

Fig. S22 The time-dependent emission spectra of **1'** upon exposure to TNT vapor.

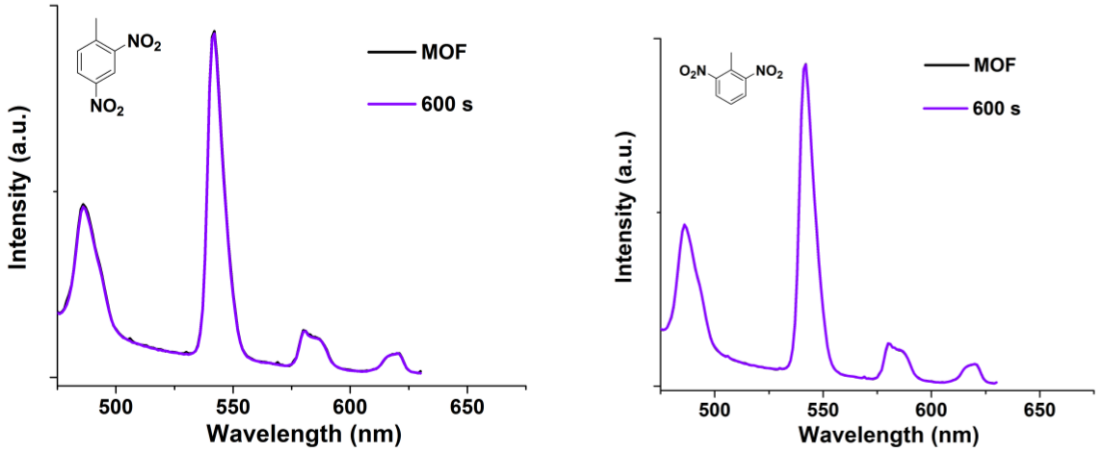

(a) (b)

Fig. S23 The time-dependent emission spectra of **1'** upon exposure to 2,4-DNT (a) and 2,6-DNT (b) vapor.

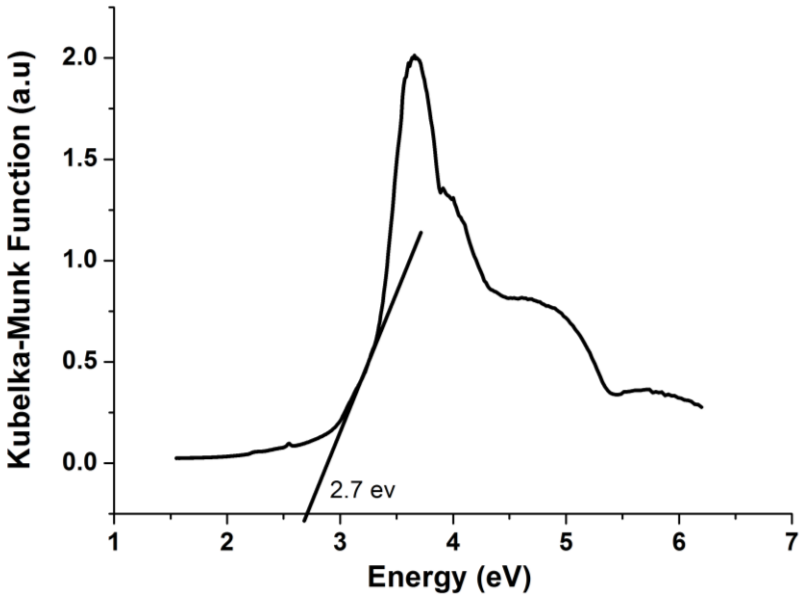

Fig. S24 The band like diffuse reflectance spectrum of a solid sample of **1'**.

The optical band gap is estimated to be ~2.7 eV.

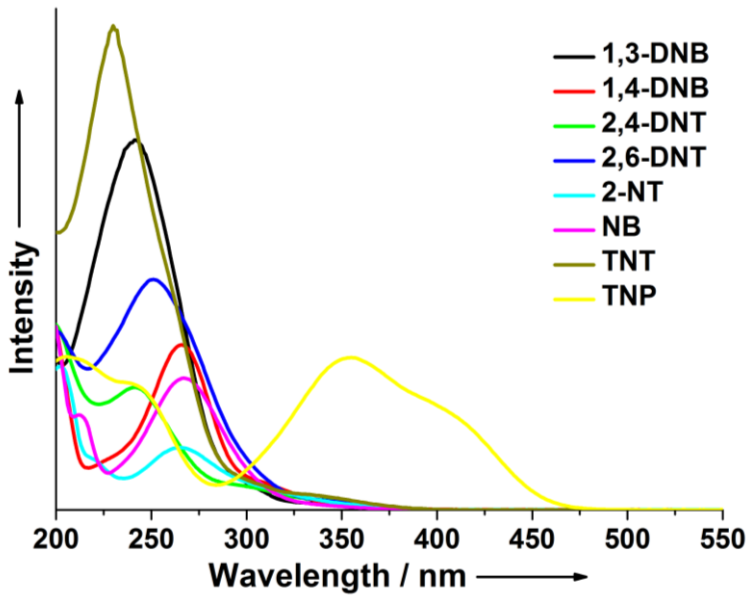

Fig. S25 The absorption spectrum of the selected analytes in water.

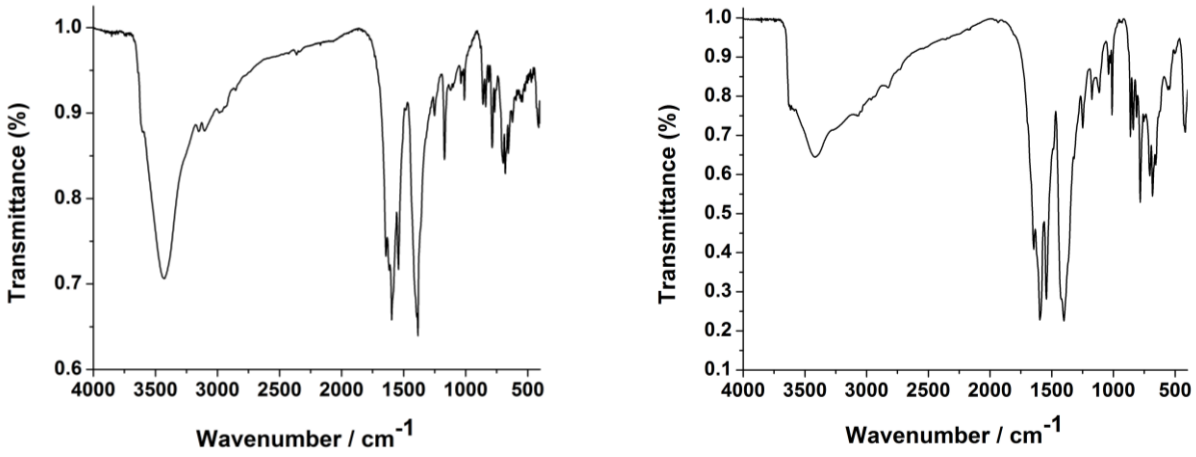

(a) (b)

Fig. S26 IR spectrum of **1** (a) and **1'** (b).

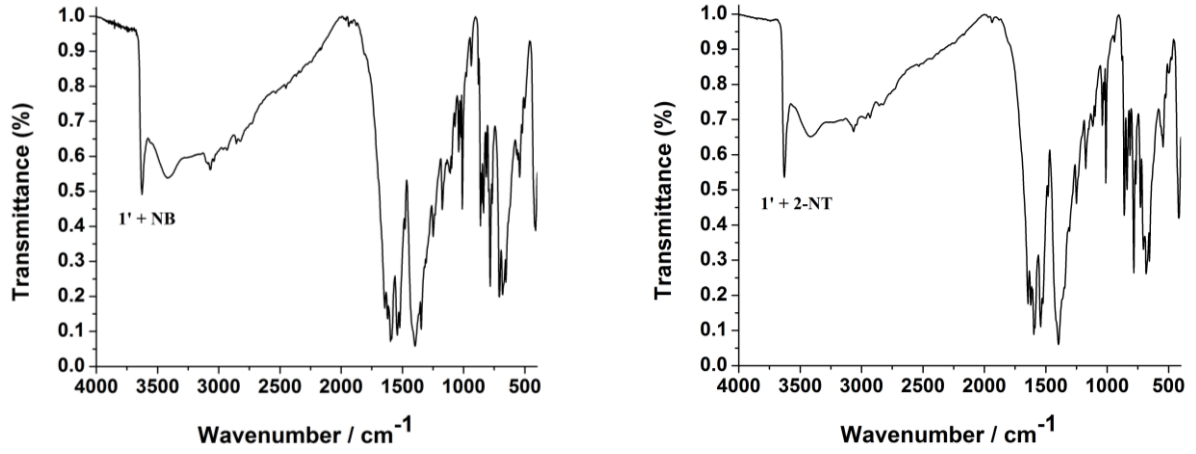

(a) (b)

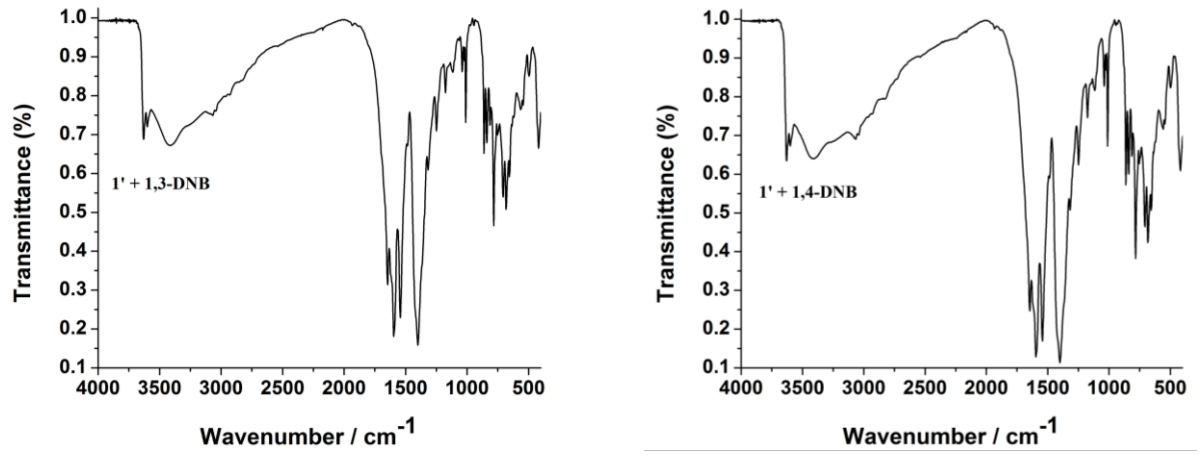

(c) (d)

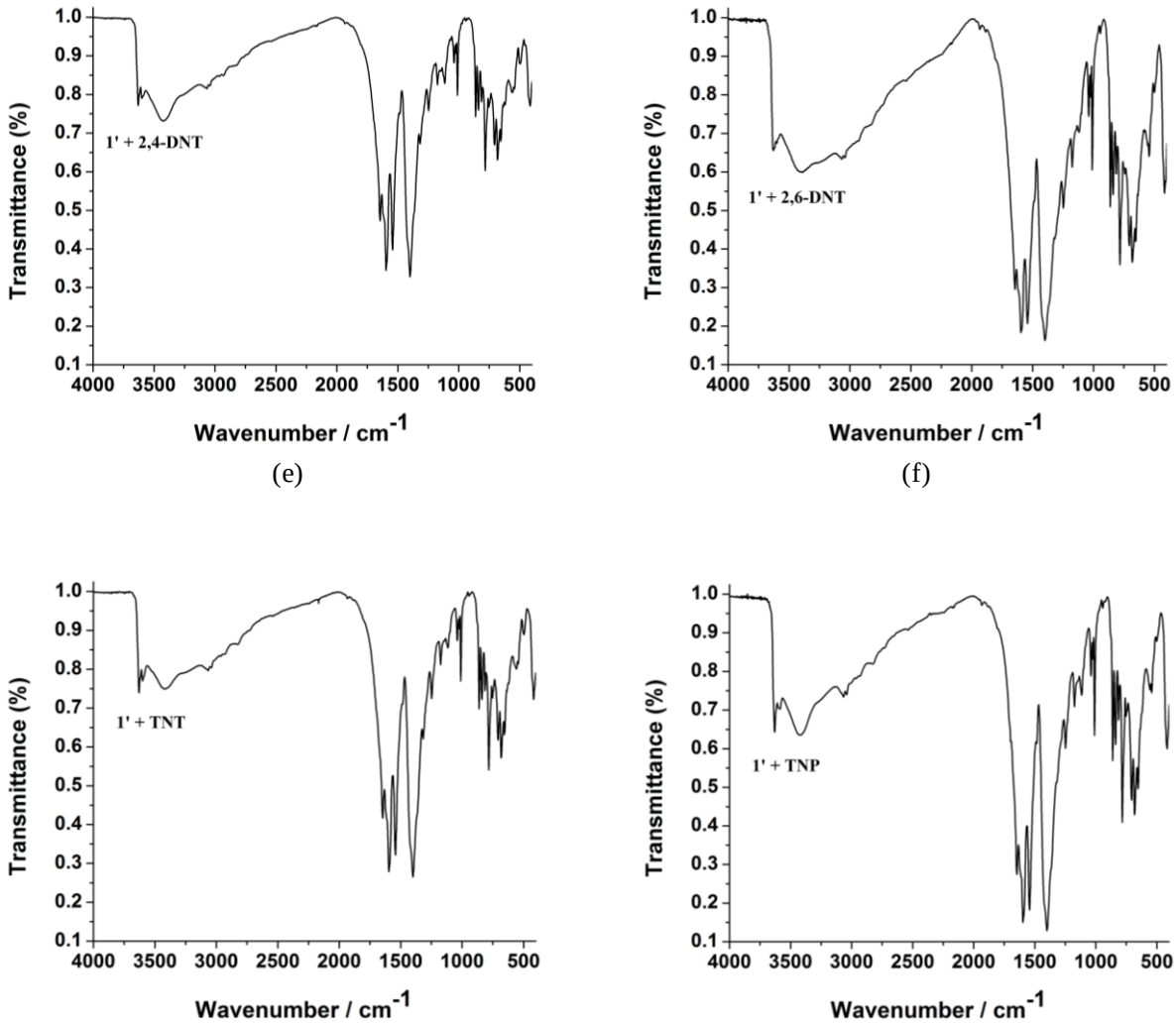

Fig. S27 IR spectrum of **1'** obtained after immersing in 1 mM or saturated aqueous solutions of the selected analytes for three days. The emerging absorption peaks in the range of 1350-1650 cm^{-1}, indicate a synergistic effect between nitro of nitroaromatic explosives and COO^{-} group of H_2L ligands.

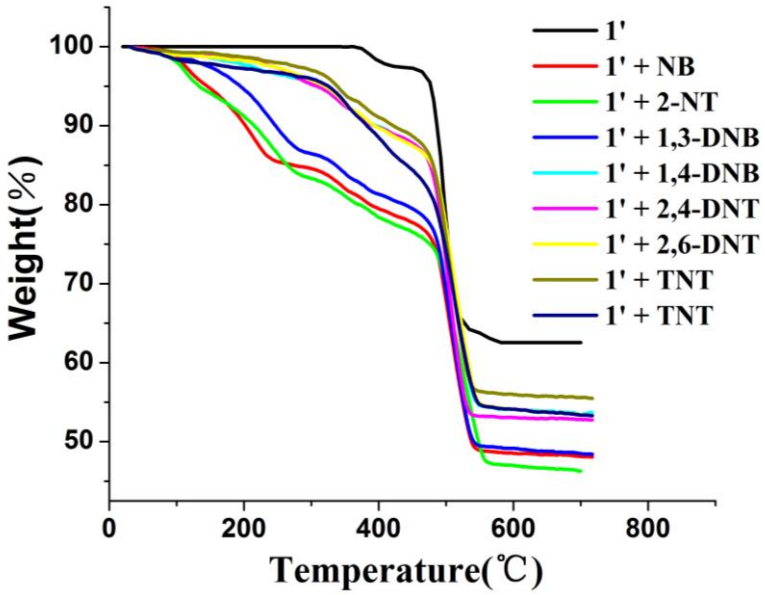

Fig. S28 Thermogravimetric curve of **1'** obtained after immersing in 1 mM or saturated aqueous solutions of the selected analytes for three days. The eight TGA curves of **1'** display a gradual weight loss of about 10% ~ 30% up to 450 ℃, which is attributed to the removal of water and nitroaromatic explosives (**Fig. S28** in ESI†).

Table S1. Crystallographic data and structure refinement detail for complex **1**.

Complexes	**1**
Formula	$C_{13}H_8NO_5Tb$
Formula weight	417.12
Crystal system	Tetragonal
Space group	*I4(1)/a*
a (Å)	30.2710(4)
b (Å)	30.2710(4)
c (Å)	8.2855(3)
α(°)	90
β(°)	90
γ(°)	90
V ($Å^3$)	7592.3(3)
Z	16
D_c (g/cm^3)	1.460
Abs coeff/mm^{-1}	3.738
F(000)	3168
θ range for data collection (°)	3.01/ 25.50
Data/restraints/parameters	3519/ 0 /181
GOF	1.079
Flack parameter	None
$R_1 = [I > 2\sigma(I)]$ [a]	0.0253
wR_2 (all data)	0.0593

$R = [\sum||F_0| - |F_d|| / \sum|F_0|]$, $R_W = \sum w [|F_0^2 - Fc^2|^2 / \sum w (|F_w|^2)^2]^{1/2}$

Table S2. Selected bond lengths (Å) and angles (°) for complex **1**.

Complex **1**			
Tb(1)-O(5)	2.347(3)	Tb(1)-O(3)#3	2.375(3)
Tb(1)-O(4)#1	2.348(3)	Tb(1)-O(5)#4	2.383(3)
Tb(1)-O(1)	2.360(3)	Tb(1)-O(2)#5	2.429(3)
Tb(1)-O(5)#2	2.364(3)	Tb(1)-N(1)	2.576(3)
O(5)-Tb(1)-O(4)#1	94.45(10)	O(3)#3-Tb(1)-O(5)#4	80.00(10)
O(5)-Tb(1)-O(1)	108.28(9)	O(5)-Tb(1)-O(2)#5	69.05(9)
O(4)#1-Tb(1)-O(1)	144.95(10)	O(4)#1-Tb(1)-O(2)#5	78.15(10)
O(5)-Tb(1)-O(5)#2	69.57(11)	O(1)-Tb(1)-O(2)#5	85.37(9)
O(4)#1-Tb(1)-O(5)#2	142.67(9)	O(5)#2-Tb(1)-O(2)#5	122.53(9)
O(1)-Tb(1)-O(5)#2	71.85(9)	O(3)#3-Tb(1)-O(2)#5	148.48(10)
O(5)-Tb(1)-O(3)#3	142.30(10)	O(5)#4-Tb(1)-O(2)#5	126.97(9)
O(4)#1-Tb(1)-O(3)#3	97.75(11)	O(5)-Tb(1)-N(1)	139.24(10)
O(1)-Tb(1)-O(3)#3	80.53(10)	O(4)#1-Tb(1)-N(1)	80.30(10)
O(5)#2-Tb(1)-O(3)#3	79.38(10)	O(1)-Tb(1)-N(1)	65.01(10)
O(5)-Tb(1)-O(5)#4	69.51(10)	O(5)#2-Tb(1)-N(1)	133.83(10)
O(4)#1-Tb(1)-O(5)#4	73.60(9)	O(3)#3-Tb(1)-N(1)	78.16(11)
O(1)-Tb(1)-O(5)#4	138.94(9)	O(5)#4-Tb(1)-N(1)	143.11(10)
O(5)#2-Tb(1)-O(5)#4	69.23(10)	O(2)#5-Tb(1)-N(1)	70.32(10)

Symmetry transformations used to generate equivalent atoms for **1**:

#1 -x, -y+2, -z; #2 -x, -y+3/2, z; #3 -y+5/4, x+3/4, z-1/4; #4 y-3/4, -x+3/4, -z-1/4; #5 -y+3/4, x+3/4, -z+3/4.

Table S3. Saturated Vapor Pressure for each of the analytes at room temperature (25 ℃).

Analytes	**Vapor Pressure (in mmHg)**	**Reduction Potential (in V *vs* SCE)**
Nitrobenzene (NB)[1]	0.2416	−1.15
2-Nitrotoluene (2-NT)[1]	0.1602	−1.2
1,3-Dinitrobenzene(1,3-DNB)[2]	8.82×10^{-4}	−0.9
1,4-Dinitrobenzene (1,4-DNB)[1]	2.406×10^{-5}	−0.7
2,4-dinitrotoluene (2,4-DNT)[1]	1.44×10^{-4}	−1.0
2,6-dinitrotoluene (2,6-DNT)[1,3]	5.61×10^{-4}	−1.0
2,4,6-trinitrotoluene (TNT)[1,4]	8.02×10^{-6}	−0.7
2,4,6-trinitrophenol (TNP)[4]	5.8×10^{-9}	−0.63

1 J. S. Yang and T. M. Swager, *J. Am. Chem. Soc*., 1998, **120**, 11864.

2 R. Hoffmann, *J. Chem. Phys.*, 1963, **39**, 1397.

3 A. J. Lan, K. H. Li, H. H. Wu, L. Z. Kong, N. Nijem, D. H. Olson, T. J. Emge, Y. J. Chabal, D. C. Langreth, M. C. Hong and J. Li, *Inorg. Chem*., 2009, **48**, 7165.

4 J. C. Sanchez and W. C. Trogler, *J. Mater. Chem*., 2008, **18**, 3143.

Table S4. Approximate sizes of the selected analytes.

Analytes	Approximate Size (D ×W ×L, Å)
NB	3.4 × 6.2 × 8.6
2-NT	5.0 × 7.7 × 8.6
1,3-DNB	5.6 × 7.7 × 8.1
1,4-DNB	5.6 × 7.7 × 9.1
2,4-DNT	5.6 × 7.7 × 10.1
2,6-DNT	5.6 × 7.7 × 9.5
TNT	5.6 × 7.7 × 10.2
TNP	5.0 × 6.2 × 7.1

Table S5. HOMO and LUMO energies calculated for H_2L and nitroaromatic explosives at B3LYP/6-31G** level of theory.

Analytes	HOMO (eV)	LUMO (eV)	Band gap
H_2L	-7.02435	-2.30916	4.71519
NB[6]	-7.5912	-2.4283	5.1629
2-NT[5]	-7.36454	-2.31722	5.04732
1,3-DNB[6]	-7.9855	-3.4311	4.5544
1,4-DNB[5]	-8.35250	-3.49679	4.85571
2,4-DNT[6]	-7.7645	-3.2174	4.5471
2,6-DNT[6]	-7.6448	-3.2877	4.3571
TNT[6]	-8.2374	-3.8978	4.3396
TNP[6]	-8.4592	-3.4926	4.9666

5 G. Y. Wang, C. Song, D. M. Kong, W. J. Ruan, Z. Chang and Y. Li, *J. Mater. Chem. A.*, 2014, **2**, 2213.

6 S. S. Nagarkar, B. Joarder, A. K. Chaudhari, S. Mukherjee and S. K. Ghosh, *Angew. Chem., Int. Ed*., 2013, **52**, 2881.